Enhancing selectivity and stability in electrochemical CO_2 reduction using tailored sputtered CuAg electrodes

Mathias van der Veer[a,b], Nick Daems[a], Pegie Cool[b], and Tom Breugelmans[a]

Supporting information

[a] Applied Electrochemistry and Catalysis (ELCAT), University of Antwerp, Campus Drie Eiken, Universiteitsplein 1, 2610 Wilrijk, Belgium

[b] Laboratory of Adsorption and Catalysis (LADCA), University of Antwerp, Campus Drie Eiken, Universiteitsplein 1, 2610 Wilrijk, Belgium

Table of content:

Fig. S1 View of in-house developed flow electrolyzer; (1) Aluminum backplate, (2) PMMA isolation plates, (3) Cathode flat graphite plate with GDE, (4) conductive copper plates, (5) Anode graphite plate with Nickel foam, (6) EPDM gaskets to seal, (7) Nafion 117 membrane, (8) Reference electrode chamber with Ag/AgCl. Flow channels for gaseous CO2, catholyte, and anolyte.

Fig. S2 Cross section FIB-SEM taken for the different CuAg samples with thicknesses measured; A) $Cu_{90}Ag_{10}$ - L, C) $Ag_{10}Cu_{90}$ - L, and E) $Cu_{90}Ag_{10}$ – CD. A top view is given for the same samples in B), D), F), where the average particle appears to be 500 nm.

Fig. S3 XPS patterns taken of sputtered Cu, and the various CuAg configurations. $Cu_{85}Ag_{15}$-L, $Cu_{85}Ag_{15}$-CD, $Ag_{15}Cu_{85}$-L, and Ag: A) Survey profiles, B) Ag 3d, C) Ag 3p, and D) Cu 2p.

Fig. S4 Contact angle measurements of A) different Cu loadings, B) $Cu_{100-x}Ag_x$ - L, C) Ag_xCu_{100-x} - L, and D) $Cu_{100-x}Ag_x$ - CD

Fig. S5 Cyclic voltammetry, measured in the flow cell with 0.5M $KHCO_3$, average taken across 5 scans, with scan rate of 50 mV s^{-}. A) various Cu loadings, B) the CuAg-L samples, C) AgCu-L samples, and D) CuAg-CD samples as compared to bare Cu and Ag.

Fig. S6 Cyclic voltammetry, measured in the flow cell with 0.5M $KHCO_3$, average taken across 5 scans, with scan rate of 50 mV s- of an Ag electrode (nomial thickness 400 nm), showing the reversible nature.

Fig. S7 Linear sweep voltammetry, measured in the flow cell with 0.5M $KHCO_3$, with scan rate of 50 mV s^{-}. A) various Cu loadings, B) CuAg-L samples, C) AgCu-L samples, and D) CuAg-CD samples as compared to bare Cu and Ag.

Fig. S8 Example of the EASA technique, CVs scanned with different scan rates ±50 mV from OCP with Cu 400 nm.

Fig. S9 Measured FEs for the different products of four distinct CuAg bimetallic catalysts at 1 hour and 150 mA cm^{-2}, Ag_5Cu_{95}-L, $Cu_{95}Ag_5$-L, $Cu_{95}Ag_5$-CD, and $Cu_{95}Ag_5Cu_{95}$-L. Error bars represent the deviation across three measurements.

Fig. S10 Measured FEs for the different products with varying CO_2 flow rate for Ag_5Cu_{95}-L at 1 hour and 150 mA cm^{-2}. Error bars represent the deviation across three measurements.

Fig. S11 Measured FEs for the different products with varying CO_2 flow rate for $Cu_{95}Ag_5$-CD at 1 hour and 150 mA cm^{-2}. Error bars represent the deviation across three measurements.

Fig. S12 The measured products FE for the different fabricated $Cu_{100-x}Ag_x$ – CD samples as compared to bare Cu and Ag. Error bars represent the deviation across three measurements.

Fig. **S13** A) CV and B) LSV comparison between bare Cu, Ag, $Cu_{99}Ag_1$-CD, $Cu_{97.5}Ag_{2.5}$-CD, and $Cu_{95}Ag_5$-CD.

Fig. S14 FIB-SEM of $Cu_{99}Ag_1$ - CD, taken after electrolysis at J =150 mA cm^{-2} for 3 hours.

Fig. S15 SEM images from top view after electrolysis of J = 150 mA cm^{-2} of the different sputtered samples, with A) Cu 400 nm, B) $Cu_{90}Ag_{10}$ - L, C) $Ag_{10}Cu_{90}$ - L, and D) $Cu_{90}Ag_{10}$ – CD.

Fig. S16 Spent GDE with graphite holding plate, water droplets have permeated through the GDE.

Fig. S17 The FE over 6 h stability measurement for respectively, A) C_2H_4, B) HER, and C) CH_4 for (black) bare $Cu_{99}Ag_1$, (red) $Cu_{99}Ag_1$ + C (50 nm), and (blue) $Cu_{99}Ag_1$ + C(400 nm). Error bars represent the deviation across three measurements.

Fig. S18 Measured FEs for the liquid products A) C_2H_5OH, B) C_3H_7OH, C) C_3H_5OH, D) $HCOO^-$, and E) CH_3COO^-, during 6 h operation for $Cu_{99}Ag_1$-CD (black), $Cu_{99}Ag_1$-CD + C (50 nm) (red), and $Cu_{99}Ag_1$-CD + C (400 nm) (blue). Error bars represent the deviation across three measurements.

Fig. S19 The FE over 6 h stability measurement for respectively, A) C_2H_4, B) HER, and C) CH_4 for (black) bare $Cu_{99}Ag_1$ (black), $Cu_{99}Ag_1$+ 0.5 mg cm^{-2} Carbon black (red), $Cu_{99}Ag_1$ + 0.5 mg cm^{-2} Carbon black + Nafion (blue), $Cu_{99}Ag_1$ + Nafion (green), $Cu_{99}Ag_1$ + 0.5 mg cm^{-2} Carbon black + Sustainion (purple), $Cu_{99}Ag_1$ + Sustainion (yellow), $Cu_{99}Ag_1$ + 0.5 mg cm^{-2} TiO_2 + Sustainion (cyan). Error bars represent the deviation across three measurements.

Fig. S20 Measured FEs for the liquid products A) C_2H_5OH, B) C_3H_7OH, C) C_3H_5OH, D) $HCOO^-$, and E) CH_3COO^-, during 6 h operation for $Cu_{99}Ag_1$ (black), $Cu_{99}Ag_1$ + 0.5 mg cm^{-2} Carbon black (red), $Cu_{99}Ag_1$ + 0.5 mg cm^{-2} Carbon black + Nafion (blue), $Cu_{99}Ag_1$ + Nafion (green), $Cu_{99}Ag_1$ + 0.5 mg cm^{-2} Carbon black + Sustainion (purple), $Cu_{99}Ag_1$ + Sustainion (yellow), and $Cu_{99}Ag_1$ + 0.5 mg cm^{-2} TiO_2 + Sustainion (cyan). Error bars represent the deviation across three measurements.

Fig. S21 Spent $Cu_{99}Ag_1$-CD with carbon black coating, after electrolysis, the carbon black is beginning to detach.

Fig. S22 During p-eCO2RR for A) Time-dependent potential 15 min of 'on' and 15 min of OCP period, B) potential response during 15 min 'on' reductive current, and C) oxidative current response when applying an oxidative pulse of -0.25 V vs Ag/AgCl for 30 s.

Fig. S23 Measured FEs for the liquid products A) C_2H_5OH, B) C_3H_7OH, C) C_3H_5OH, D) $HCOO^-$, and E) CH_3COO^-, during 6 h operation for $Cu_{99}Ag_1$ at continuous operation (black), Pulsed: 15 min operation + 15 min OCP (red), and Pulsed: 15 min operation + 30 s at -0.25 V vs Ag/AgCl (blue). Error bars represent the deviation across three measurements.

Table S1. Overview of the prepared electrodes with the setpoint (SP) and the deposition rate (Å/s) used during sputtering.

Table S2. Reported loadings of Cu on the different thicknesses.

Table S3. ICP-MS results for the different CuAg composites.

Table S4. Calculated C_{dl} of Cu on the different thicknesses.

Table S5. Average measured potentials (V) of Cu on the different thicknesses vs Ag/AgCl during 1 h chronopotentiometry at J = 150 mA cm^{-2}.

Table S6. Average measured potentials (V) of CuAg composites vs Ag/AgCl during 1 h chronopotentiometry at J = 150 mA cm^{-2}.

Table S7. Overview of recently reported CuAg bimetallic catalysts for the eCO_2RR to C_{2+} products.

Table S8. The measured C_{dl} of before and after electrolysis with the different $Cu_{100-x}Ag_x$ samples.

Methods

Electrode preparation

The magnetron sputter coater (Moorfield Lab125) is equipped with 3 target positions, i.e. a DC, pulsed DC and RF type, which are respectively linked to two 1500W (TDK-Lambda) and a 600W (Seren) power sources. The substrate plate inside the 125 L compartment is liquid cooled at 20°C (SMC) and rotates up to 10 rpm during sputtering. A dry scroll pump and turbopump (Edwards) bring the sputtering compartment to a vacuum down to 10^{-6} Pa. The deposition unit (Infinicon SQC-310C) regulates the shutters, gas pressure and power of the sources according to a preprogrammed protocol to automate the deposition.

Physiochemical characterisation

Primarily, a protective layer of platinum was deposited (by ion beam induced Pt deposition at 30 kV with a beam current of 0.23 nÅ) on the film in order to (1) prevent beam damage and (2) allow correct measurement of the film thickness. Thereafter, part of the sample was milled using a focused ion beam to provide a cross-section view.

Flow cell configuration

The working electrode (2 cm^2) rests on a flat designed graphite plate and consists of the prepared GDE samples, with electrical contact on the backside of the graphite plates (for cathode and anode) provided via a copper current collector, as described previously(8). Ag/AgCl (sat. KCl) was used as the reference electrode, to control the cathodic potential, and a nickel foam as the counter electrode. Chronopotentiometric electrolysis was performed using high purity CO_2 (99.996%), which was continuously fed through the electrolyser at a rate of 15 sccm by a mass flow controller. The cathodic and anodic chamber were separated by a Nafion® 117 membrane. The anolyte, 2 M KOH, was recycled over the Ni foam at a flow rate of 2.6 mL min^{-1}. The catholyte stream, e.g. 0.5 M $KHCO_3$ (pH ≈ 8.5), was circulated (single-pass) through the cathodic chamber at a flow rate of 2.6 mL min^{-1} (Figure S1). All experiments were repeated three times for reproducibility and at room temperature. The collected liquid samples were subsequently analysed with GC-FID and HPLC for the detection of alcohols, acetic, and formic acid. For the alcohols, a mixture of standard solutions (1000 ppm) was prepared for ethanol, propanol, and allyl alcohol. A mixture was prepared in a vial with 100 µL of each standard mixed with 100 µL of butanol (internal standard), and 600 µL of MQ water and the vials were vortexed to assure an optimal, homogenous solution. The measured samples were prepared by adding 100 µL of butanol to 900 µL sample and they were vortexed again prior to analysis.

The HPLC was used for the detection of acetic and formic acid, samples were prepared by filtrating 900 µL of liquid product with 900 µL $HClO_4$ (1.2 M) to precipitate the catholyte salts, the resulting liquid was collected in a vial and analysed together with a formic acid standard of 1000 ppm.

Finally, to evaluate the catalytic performance, faradaic efficiencies (FEs) of the liquid and gaseous products were determined according to the following equations:

$$FE\% = 100 * \frac{n * F * C * V}{Q}$$

$$FE\% = 100 * \frac{n * F * C * v * P}{R * T * l}$$

Here, n represents the number of electrons exchanged, F the faraday constant 96485 A*s mol^{-1}, C denotes the concentration of the product, V the amount of electrolyte, Q the charge given in A*s, v the gas flow rate in mL min^{-1}, P = 101.325 kPa, R = 8.314 J $(mol*K)^{-1}$, T = 298 K and l the applied current (A).

$$EE\% = 100 * \frac{FE * E_{theoritical}}{E_{experimental}}$$

$E_{Theoritical}$ is the difference of the water oxidation potential (1.23 V vs RHE) and the standard reduction potential of CO_2 → C_2H_4 (0.065 V vs RHE) or CO_2 → C_2H_5OH (0.085 V vs RHE). The $E_{experimental}$ is the difference between the water oxidation potential and the measured cathodic overpotential.

In those cases that the total FE doesn't reach 100%, the missing FE can be attributed to either some evaporation of volatile products, or due to the multiproduct analysis, a higher degree of errors is noticed, as no crossover products were detected in the anolyte. Furthermore, some current is directed to the reduction of the catalyst itself. We are therefore confident that no relevant products are lost and our analysis of the results remains valid even for those cases.
All measured potentials were converted to the reversible hydrogen electrode (RHE) scale according to the Nernst equation shown in *eq.1*: where 0.199 V corresponds to the value relative to the standard reduction potential of Ag/AgCl (sat. KCl).

$$E\ (RHE) = E\left(\frac{Ag}{AgCl}\right) + 0.199\ V + 0.059 * pH$$

Experimental results

Electrochemical active surface area

When comparing different catalysts, the electrochemical active surface area (EASA) is a useful metric in comparing activity (see **Fig. S8**), as suggested in our previous work.[1] In this study, we observe that the roughness factor increases with Cu loading (**Table S4**), however, as we will discuss in section 3.3, this has little effect on the intrinsic activity (**Table S5**, for measured overpotentials) of the different samples as the activity towards eCO_2RR remains similar. Related to this, no real correlation between the roughness factor of the different CuAg samples and its activity could be observed (see also section 3.3). For this reason, we believe the relevance of using EASA is limited to the comparison of different structured catalysts and less so for layers of Cu, Ag or a combination of CuAg where the roughness is largely determined by the substrate and the impact of EASA on performance is less important than its composition. This was also confirmed by a previous study with sputtered materials, where the EASA of Cu and CuAg materials resulted in only 0.1 mF difference but the activity towards C_{2+} was substantially enhanced.[2]

References

1. Van Der Veer M, Daems N, Cool P, Breugelmans T. From batch to flow: the effect of pH, current, and the crystal facets of Cu $_2$ O on electrochemical CO $_2$ reduction. Sustainable Energy Fuels. 2024;8(11):2504–18.

2. Li YC, Wang Z, Yuan T, Nam DH, Luo M, Wicks J, et al. Binding Site Diversity Promotes CO2 Electroreduction to Ethanol. J Am Chem Soc. 2019 May 29;141(21):8584–91.

Table S1. Overview of the prepared electrodes with the setpoint (SP) and the deposition rate (Å/s) used during sputtering.

Sample	Cu SP (kÅ)	Cu rate (Å/s)	Ag SP (kÅ)	Ag rate (Å/s)
Cu – 50 nm	0.856	5.3	n.a.	n.a.
Cu – 100 nm	1.701	5.3	n.a.	n.a.
Cu – 150 nm	2.533	5.3	n.a.	n.a.
Cu – 200 nm	3.354	5.3	n.a.	n.a.
Cu – 300 nm	4.959	5.3	n.a.	n.a.
Cu – 400 nm	6.515	5.3	n.a.	n.a.
Cu – 500 nm	8.023	5.3	n.a.	n.a.
Cu – 600 nm	9.483	5.3	n.a.	n.a.
Cu – 700 nm	10.900	5.3	n.a.	n.a.
Cu – 800 nm	12.260	5.3	n.a.	n.a.
Ag – 400 nm	n.a.	n.a.	9.231	3
$Cu_{95}Ag_5$ – L	6.207	5.3	0.462	3
$Cu_{90}Ag_{10}$ – L	5.900	5.3	0.923	3
$Cu_{85}Ag_{15}$ – L	5.587	5.3	1.385	3
$Cu_{80}Ag_{20}$ – L	5.273	5.3	1.846	3
$Cu_{99}Ag_1$ – CD	6.420	7.8	0.0649	0.08
$Cu_{97.5}Ag_{2.5}$ – CD	6.254	5.3	0.231	0.2
$Cu_{95}Ag_5$ – CD	6.207	5.3	0.462	0.39
$Cu_{90}Ag_{10}$ – CD	5.900	5.3	0.923	0.83
$Cu_{85}Ag_{15}$ – CD	5.587	5.3	1.385	1.31
$Cu_{80}Ag_{20}$ – CD	5.273	5.3	1.846	1.86
$Cu_{70}Ag_{30}$ – CD	4.614	5.3	2.77	3.18
$Cu_{60}Ag_{40}$ – CD	3.955	5.3	3.693	4.95
$Cu_{50}Ag_{50}$ – CD	3.296	5.3	4.617	7.42
$Cu_{40}Ag_{60}$ – CD	2.637	5.3	5.539	11.13
$Cu_{30}Ag_{70}$ – CD	1.977	5.3	6.463	17.3
Ag_5Cu_{95} – L	6.207	5.3	0.462	3
$Ag_{10}Cu_{90}$ -L	5.900	5.3	0.923	3
$Ag_{15}Cu_{85}$ – L	5.587	5.3	1.385	3
$Ag_{20}Cu_{80}$ – L	5.273	5.3	1.846	3

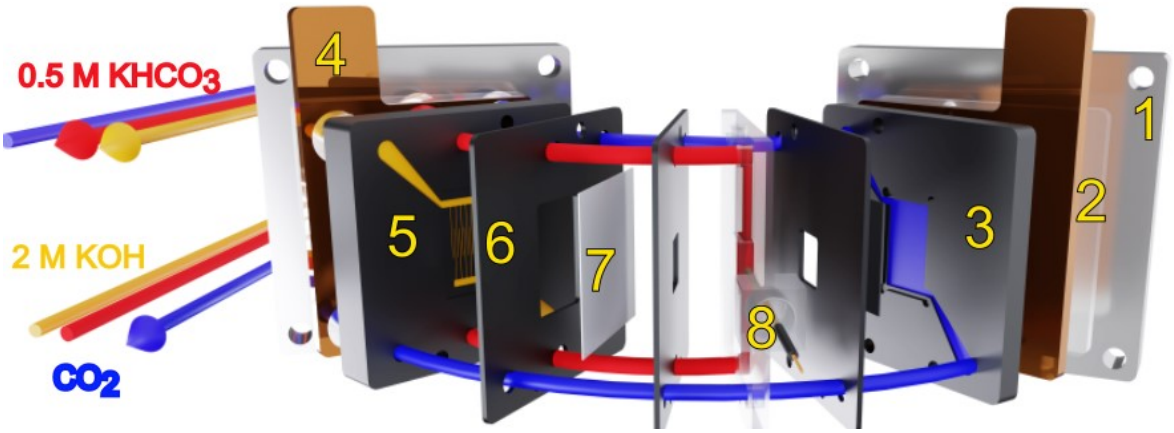

Fig. S1 View of in-house developed flow electrolyzer; (1) Aluminum backplate, (2) PMMA isolation plates, (3) Cathode flat graphite plate with GDE, (4) conductive copper plates, (5) Anode graphite plate with Nickel foam, (6) EPDM gaskets to seal, (7) Nafion 117 membrane, (8) Reference electrode chamber with Ag/AgCl. Flow channels for gaseous CO_2, catholyte, and anolyte.

Table S2. Reported loadings of Cu on the different thicknesses.

Sample	Loading (μg cm^{-2})	Sample	Loading (μg cm^{-2})
Cu$_{50\ nm}$	47	**Cu$_{400\ nm}$**	340
Cu$_{100\ nm}$	93	**Cu$_{500\ nm}$**	507
Cu$_{150\ nm}$	139	**Cu$_{600\ nm}$**	597
Cu$_{200\ nm}$	168	**Cu$_{700\ nm}$**	665
Cu$_{300\ nm}$	287	**Cu$_{800\ nm}$**	784

Table S3. ICP-MS results for the different CuAg composites.

Sample	Cu%	Ag%	**Sample**	Cu%	Ag%	**Sample**	Cu%	Ag%
$Cu_{80}Ag_{20}$-L	77.1	22.9	**$Cu_{80}Ag_{20}$-CD**	79.1	20.9	**$Ag_{20}Cu_{80}$-L**	76.6	23.4
$Cu_{85}Ag_{15}$-L	82.2	17.8	**$Cu_{85}Ag_{15}$-CD**	83.7	16.3	**$Ag_{15}Cu_{85}$-L**	81.9	18.1
$Cu_{90}Ag_{10}$-L	86.8	13.2	**$Cu_{90}Ag_{10}$-CD**	87.3	12.7	**$Ag_{10}Cu_{90}$-L**	87.1	12.9
$Cu_{95}Ag_{5}$-L	92.7	7.36	**$Cu_{95}Ag_{5}$-CD**	93.4	6.6	**$Ag_{5}Cu_{95}$-L**	92.6	7.4
			$Cu_{97.5}Ag_{2.5}$-CD	96.8	3.2			
			$Cu_{99}Ag_{1}$-CD	98.7	1.3			
			$Cu_{70}Ag_{30}$-CD	69.2	30.8			
			$Cu_{60}Ag_{40}$-CD	58.8	41.2			
			$Cu_{50}Ag_{50}$-CD	49.1	50.9			
			$Cu_{40}Ag_{60}$-CD	38.6	61.4			
			$Cu_{30}Ag_{70}$-CD	28.7	71.3			

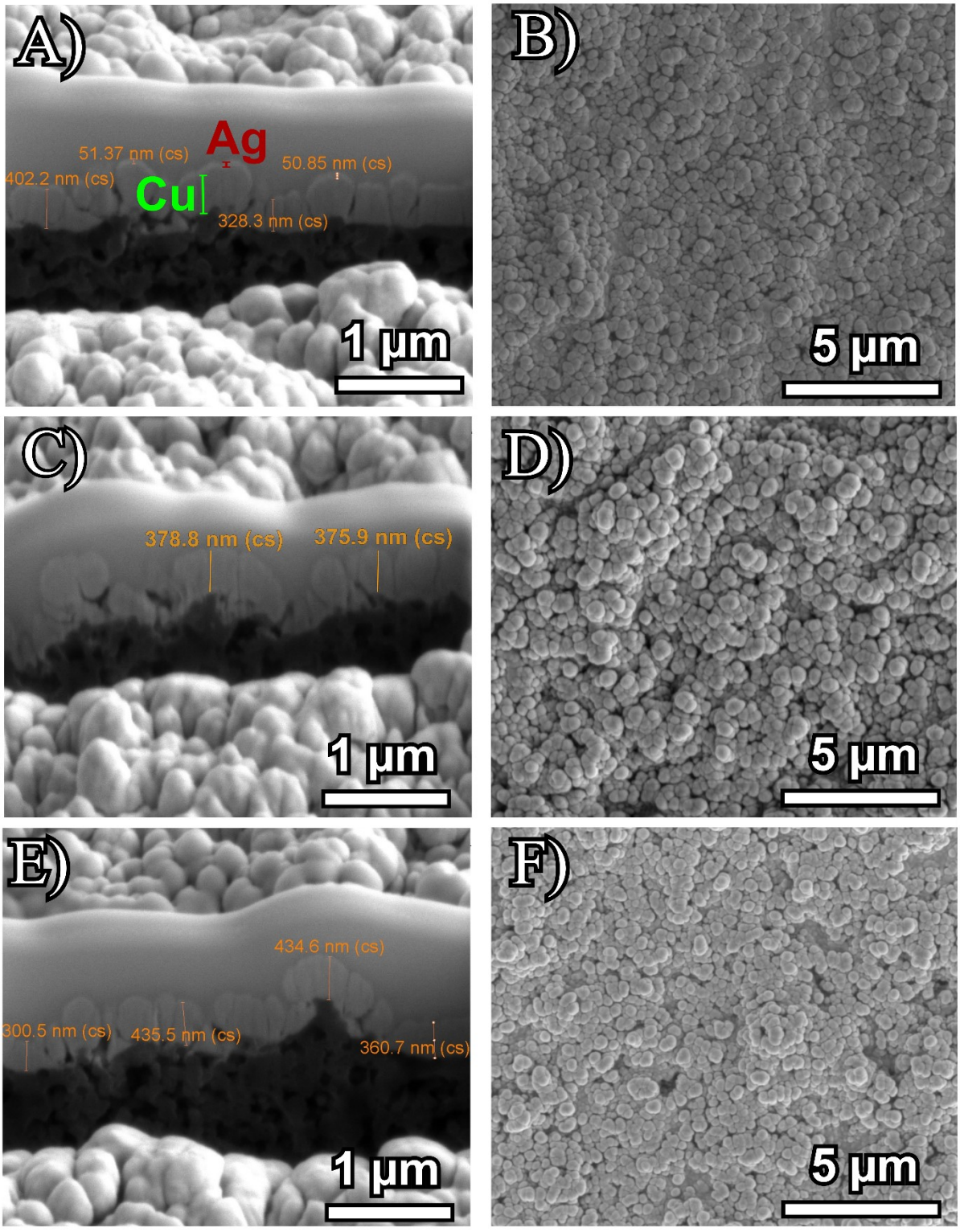

Fig. S2 Cross section FIB-SEM taken for the different CuAg samples with thicknesses measured; A) $Cu_{90}Ag_{10}$ - L, C) $Ag_{10}Cu_{90}$ - L, and E) $Cu_{90}Ag_{10}$ – CD. A top view is given for the same samples in B), D), F), where the average particle appears to be 500 nm.

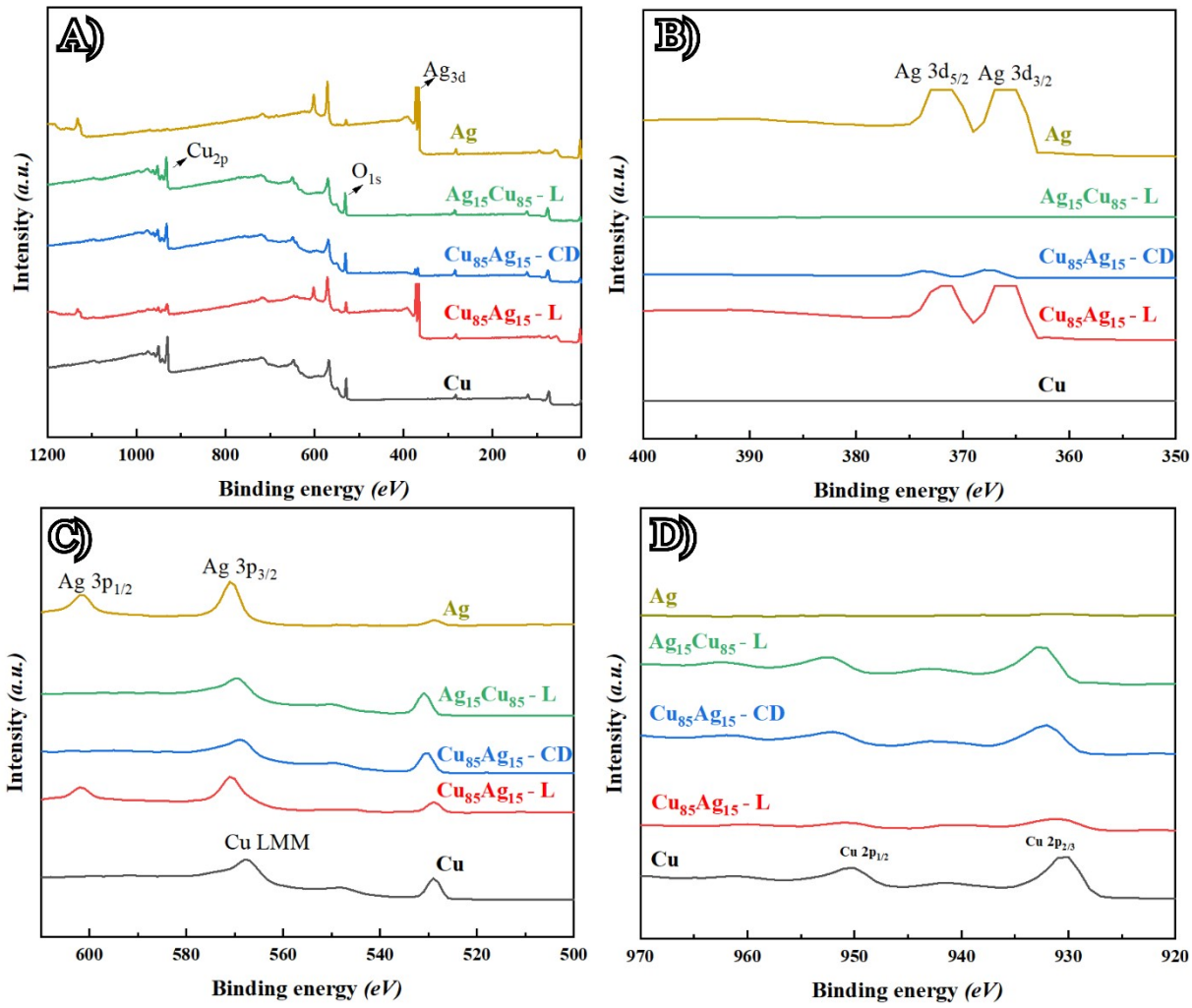

Fig. S3 XPS patterns taken of sputtered Cu, and the various CuAg configurations. $Cu_{85}Ag_{15}$-L, $Cu_{85}Ag_{15}$-CD, $Ag_{15}Cu_{85}$-L, and Ag: A) Survey profiles, B) Ag 3d, C) Ag 3p, and D) Cu 2p.

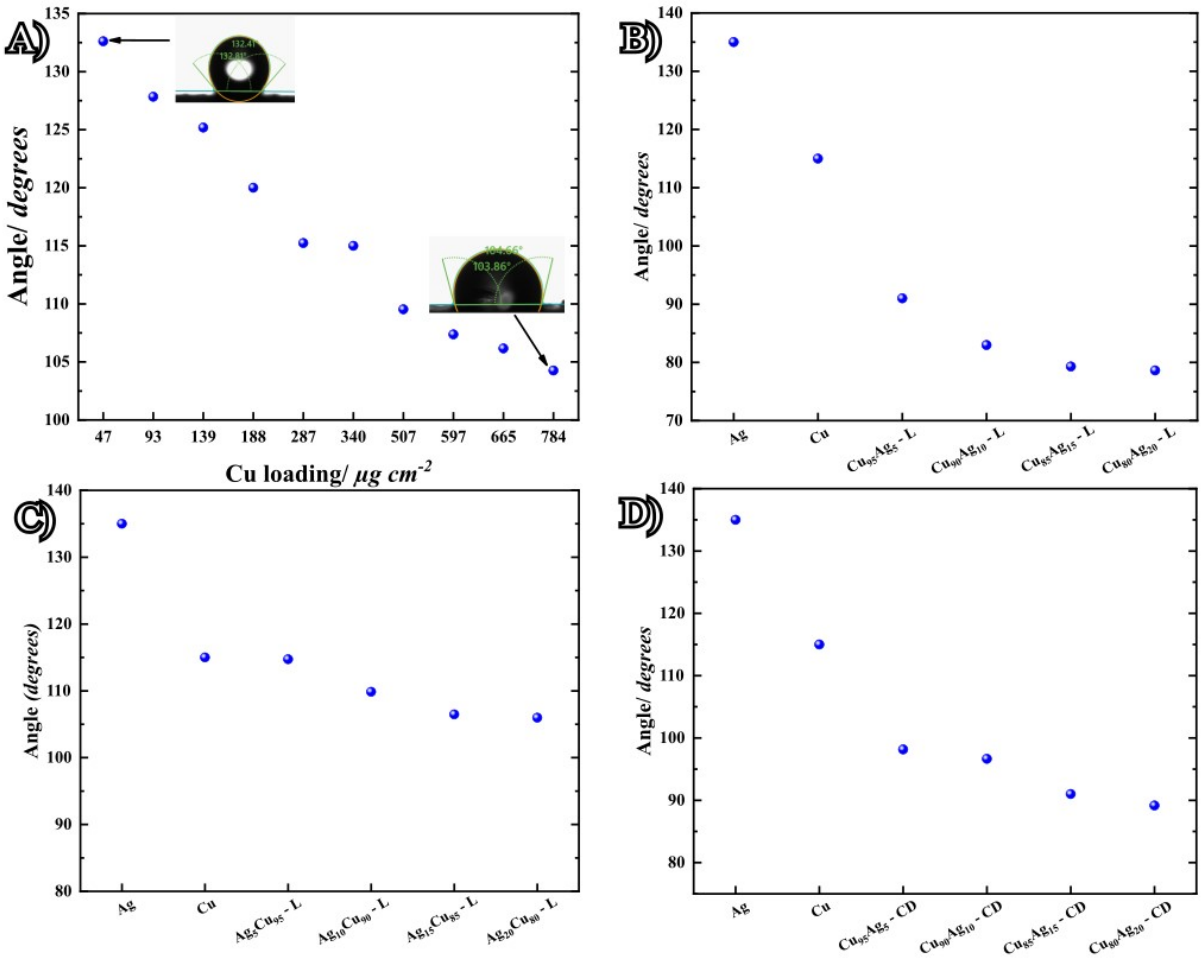

Fig. S4 Contact angle measurements of A) different Cu loadings, B) $Cu_{100-x}Ag_x$ - L, C) Ag_xCu_{100-x} - L, and D) $Cu_{100-x}Ag_x$ - CD

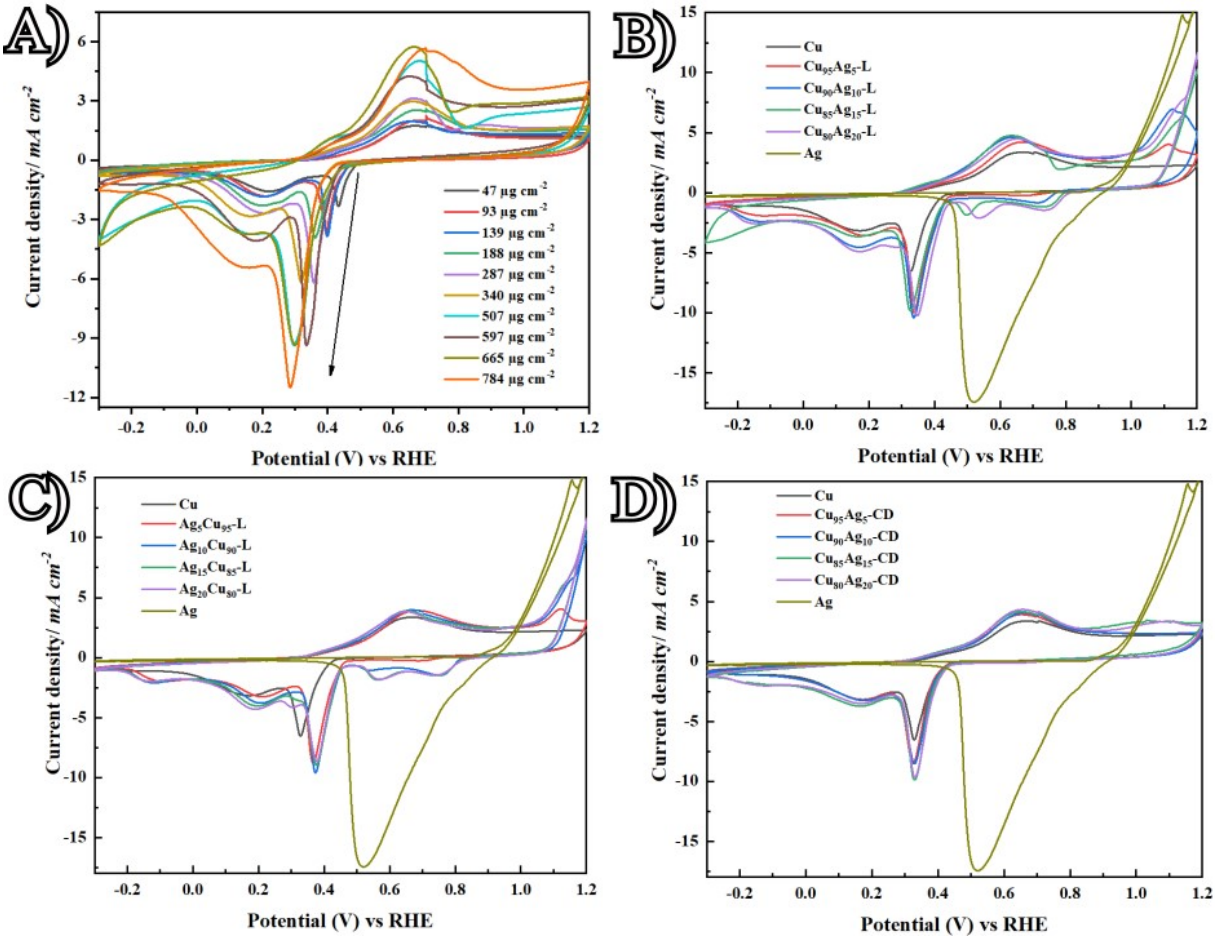

Fig. S5 Cyclic voltammetry, measured in the flow cell with 0.5M $KHCO_3$, average taken across 5 scans, with scan rate of 50 mV s^{-}. A) various Cu loadings, B) the CuAg-L samples, C) AgCu-L samples, and D) CuAg-CD samples as compared to bare Cu and Ag.

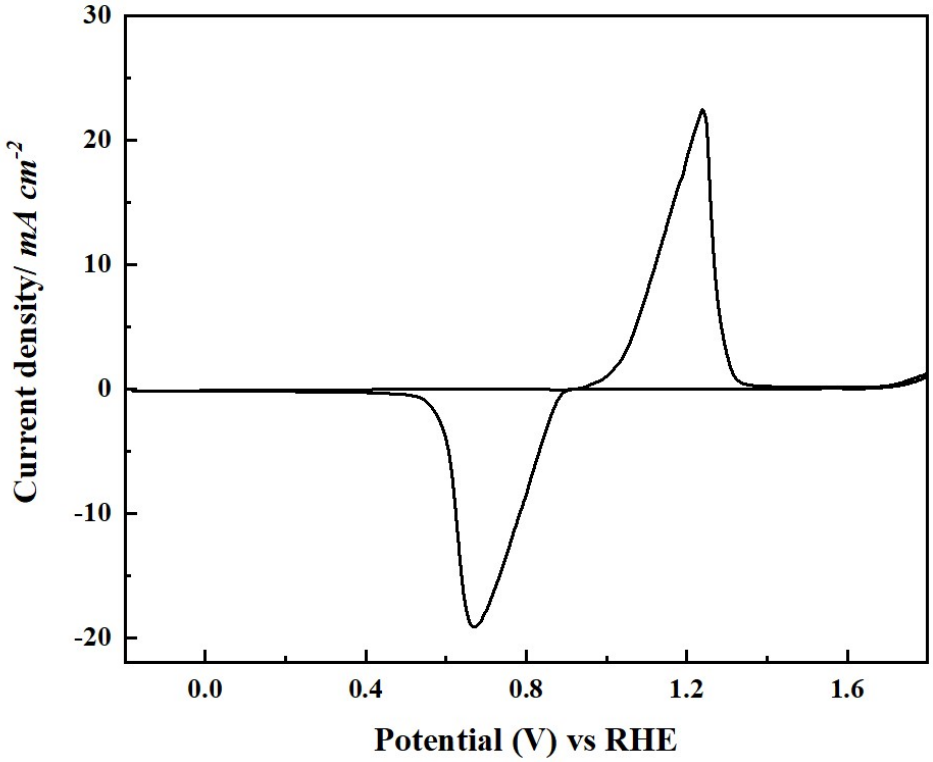

Fig. S6 Cyclic voltammetry, measured in the flow cell with 0.5M KHCO3, average taken across 5 scans, with scan rate of 50 mV s- of an Ag electrode (nominal thickness 400 nm), showing the reversible nature.

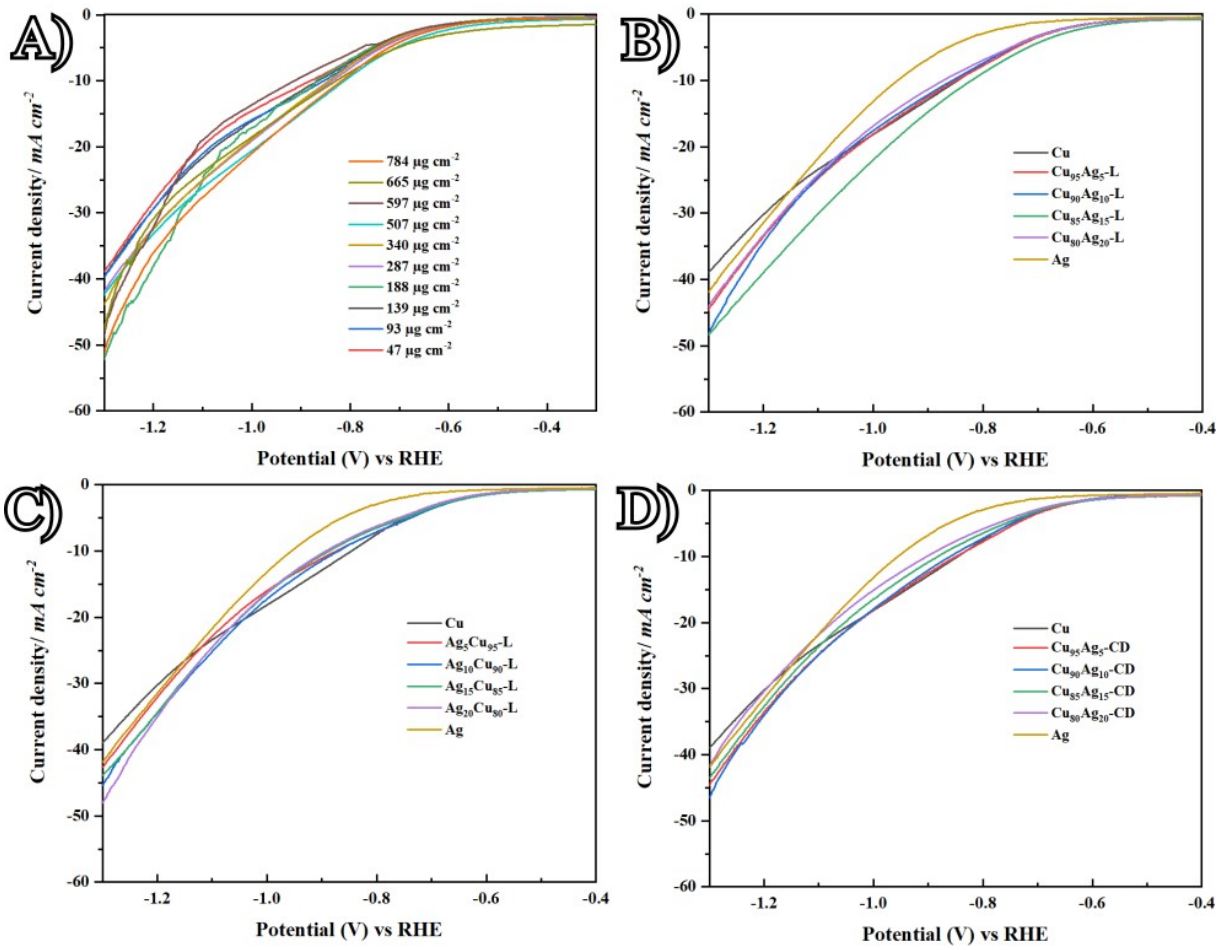

Fig. S7 Linear sweep voltammetry, measured in the flow cell with 0.5M $KHCO_3$, with scan rate of 50 mV s^{-}. A) various Cu loadings, B) CuAg-L samples, C) AgCu-L samples, and D) CuAg-CD samples as compared to bare Cu and Ag.

Table S4. Calculated Cdl of Cu on the different thicknesses.

Sample	C_{dl} (mF) before	C_{dl} (mF) after	Sample	C_{dl} (mF) before	C_{dl} (mF) after
$Cu_{50\ nm}$	0.37	**1.16**	**$Cu_{400\ nm}$**	1.61	2.54
$Cu_{100\ nm}$	0.53	**1.18**	**$Cu_{500\ nm}$**	1.79	3.04
$Cu_{150\ nm}$	0.57	**1.25**	**$Cu_{600\ nm}$**	1.98	3.10
$Cu_{200\ nm}$	0.85	**1.78**	**$Cu_{700\ nm}$**	2.31	3.15
$Cu_{300\ nm}$	1.17	**1.89**	**$Cu_{800\ nm}$**	2.8	3.64

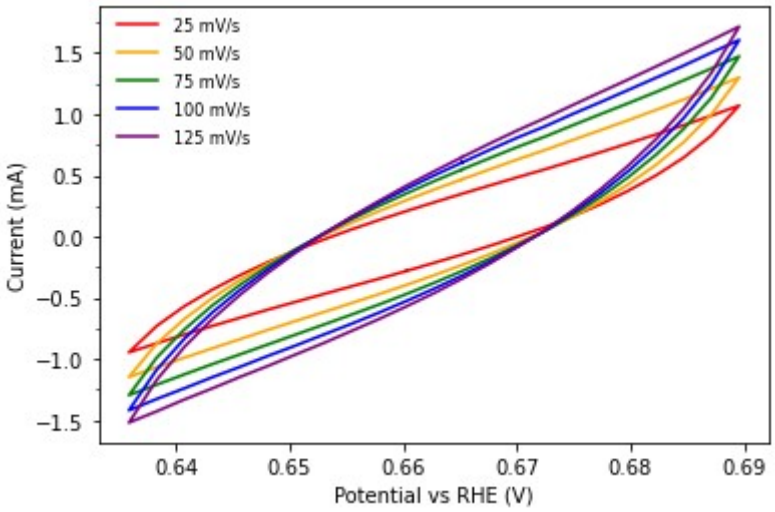

Fig. S8 Example of the EASA technique, CVs scanned with different scan rates ± 50 mV from OCP with Cu 400 nm.

Table S5. Average measured potentials (V) of Cu on the different thicknesses vs Ag/AgCl during 1 h chronopotentiometry at $J = 150$ mA cm^{-2}.

Sample	V vs Ag/AgCl	Sample	V vs Ag/AgCl
$\mathbf{Cu_{50\ nm}}$	-2.57	$\mathbf{Cu_{400\ nm}}$	-2.52
$\mathbf{Cu_{100\ nm}}$	-2.56	$\mathbf{Cu_{500\ nm}}$	-2.54
$\mathbf{Cu_{150\ nm}}$	-2.58	$\mathbf{Cu_{600\ nm}}$	-2.61
$\mathbf{Cu_{200\ nm}}$	-2.54	$\mathbf{Cu_{700\ nm}}$	-2.65
$\mathbf{Cu_{300\ nm}}$	-2.60	$\mathbf{Cu_{800\ nm}}$	-2.63

Table S6. Average measured potentials (V) of CuAg composites vs Ag/AgCl during 1 h chronopotentiometry at J = 150 mA cm^{-2}.

Sample	V vs Ag/AgCl	Sample	V vs Ag/AgCl	Sample	V vs Ag/AgCl
$Cu_{99}Ag_1$ - CD	-2.43	**$Cu_{95}Ag_5$ - L**	-2.54	**Ag_5Cu_{95} - L**	-2.58
$Cu_{97.5}Ag_{2.5}$ - CD	-2.57	**$Cu_{90}Ag_{10}$ - L**	-2.61	**$Ag_{10}Cu_{90}$ - L**	-2.57
$Cu_{95}Ag_5$ - CD	-2.56	**$Cu_{85}Ag_{15}$ - L**	-2.63	**$Ag_{15}Cu_{85}$ - L**	-2.62
$Cu_{90}Ag_{10}$ - CD	-2.58	**$Cu_{80}Ag_{20}$ - L**	-2.58	**$Ag_{20}Cu_{80}$ - L**	-2.64
$Cu_{85}Ag_{15}$ - CD	-2.61			**Ag**	-2.71
$Cu_{80}Ag_{20}$ - CD	-2.62				

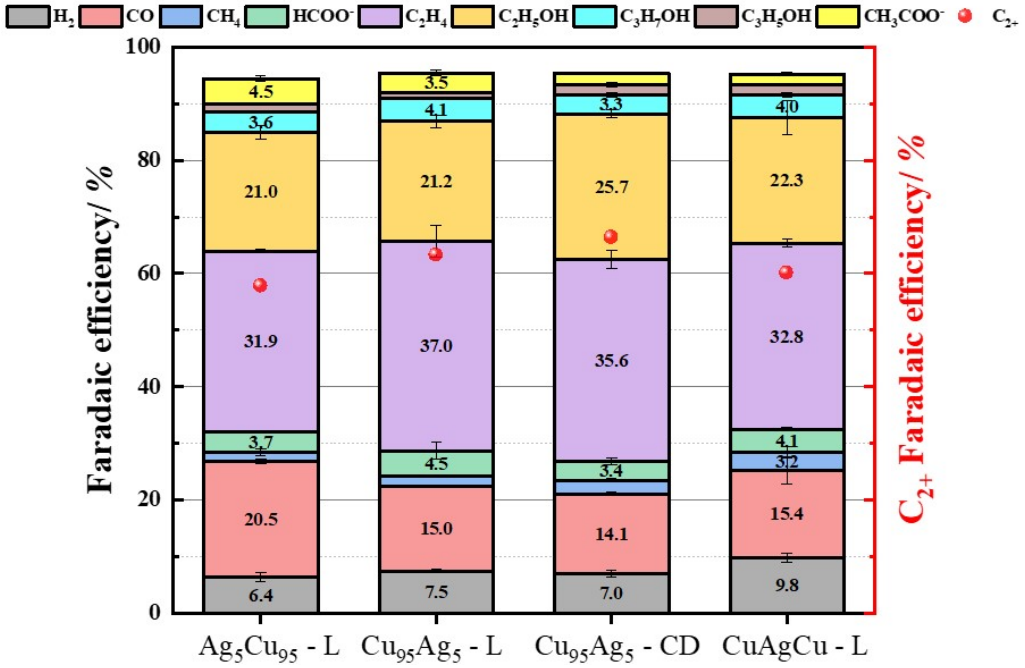

Fig. S9 Measured FEs for the different products of four distinct CuAg bimetallic catalysts at 1 hour and 150 mA cm^{-2}, Ag_5Cu_{95}-L, $Cu_{95}Ag_5$-L, $Cu_{95}Ag_5$-CD, and $Cu_{95}Ag_5Cu_{95}$-L. Error bars represent the deviation across three measurements.

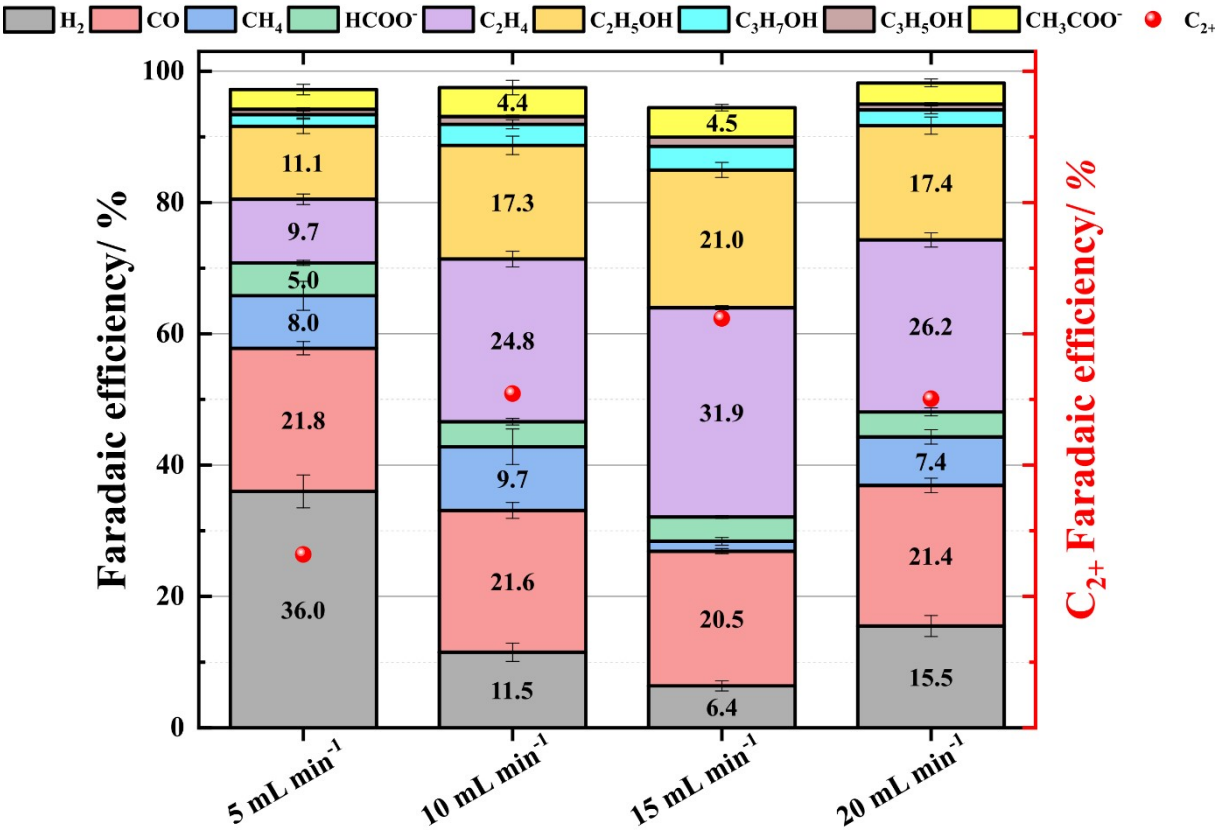

Fig. S10 Measured FEs for the different products with varying CO_2 flow rate for Ag_5Cu_{95}-L at 1 hour and 150 mA cm^{-2}. Error bars represent the deviation across three measurements.

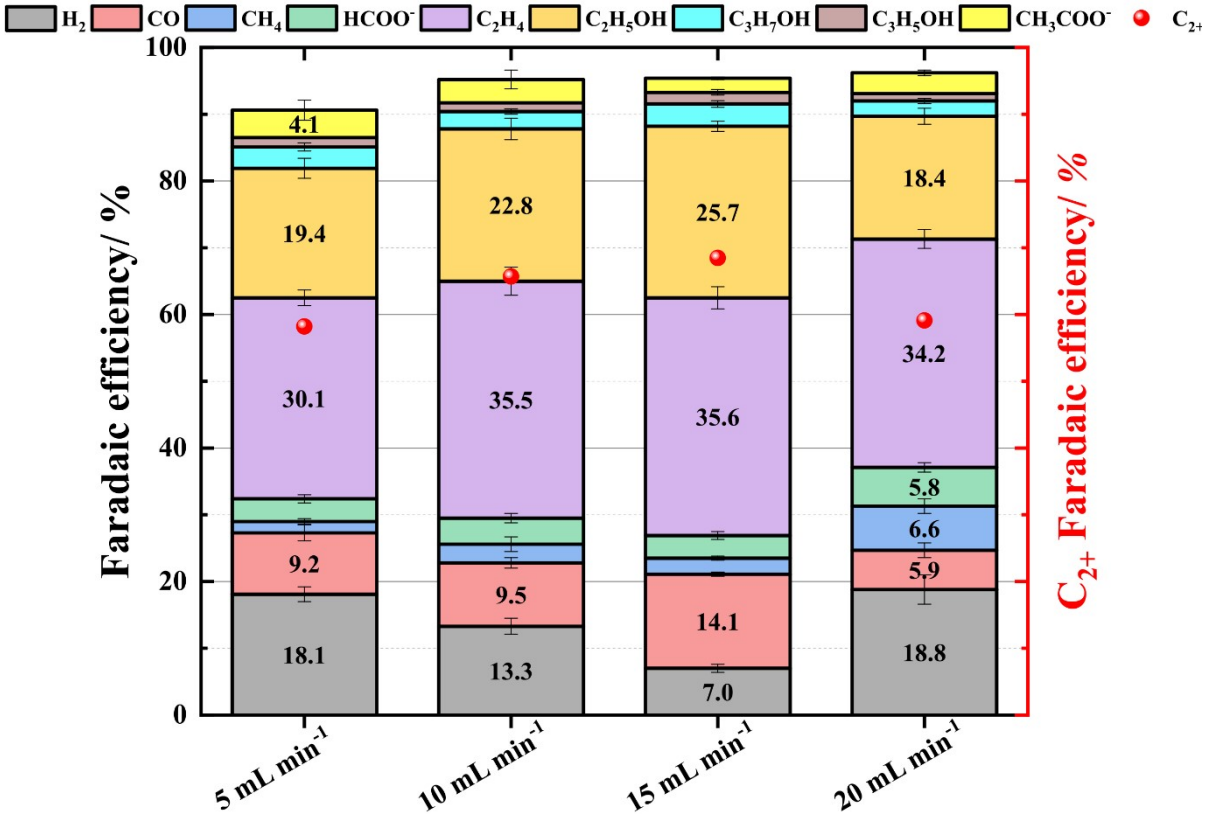

Fig. S11 Measured FEs for the different products with varying CO_2 flow rate for $Cu_{95}Ag_5$-CD at 1 hour and 150 mA cm^{-2}. Error bars represent the deviation across three measurements.

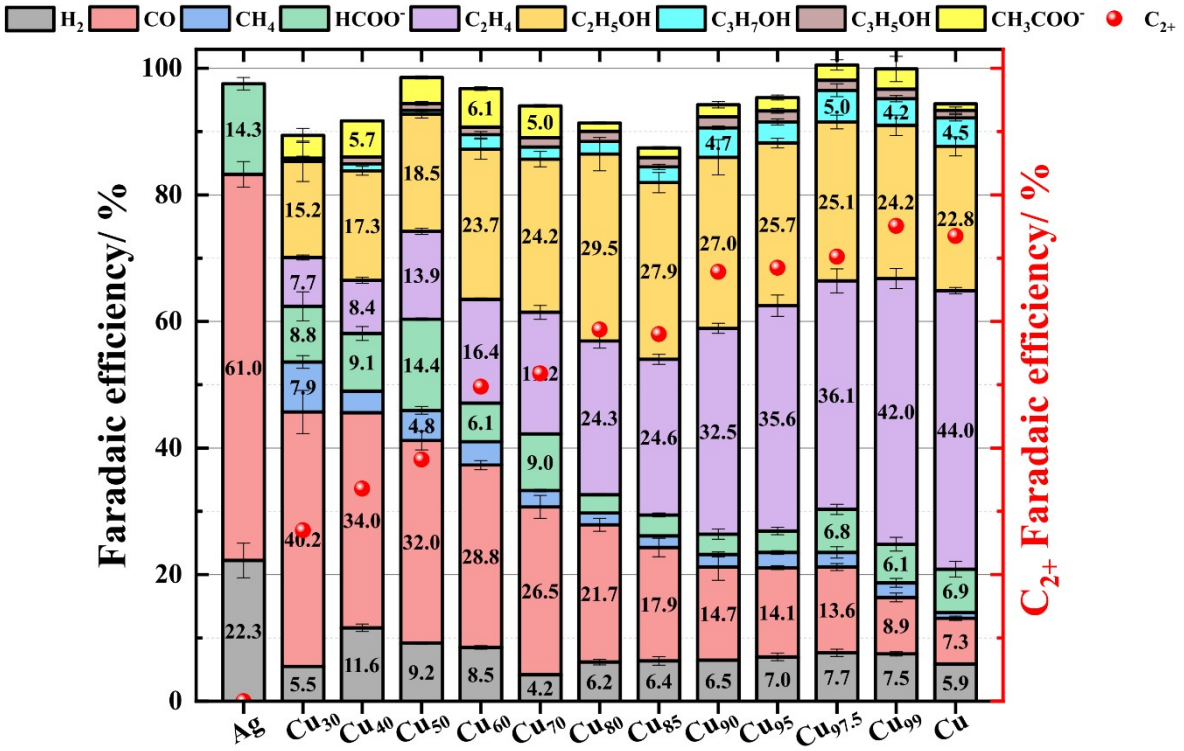

Fig. S12 The measured products FE for the different fabricated $Cu_{100-x}Ag_x$ – CD samples as compared to bare Cu and Ag. Error bars represent the deviation across three measurements.

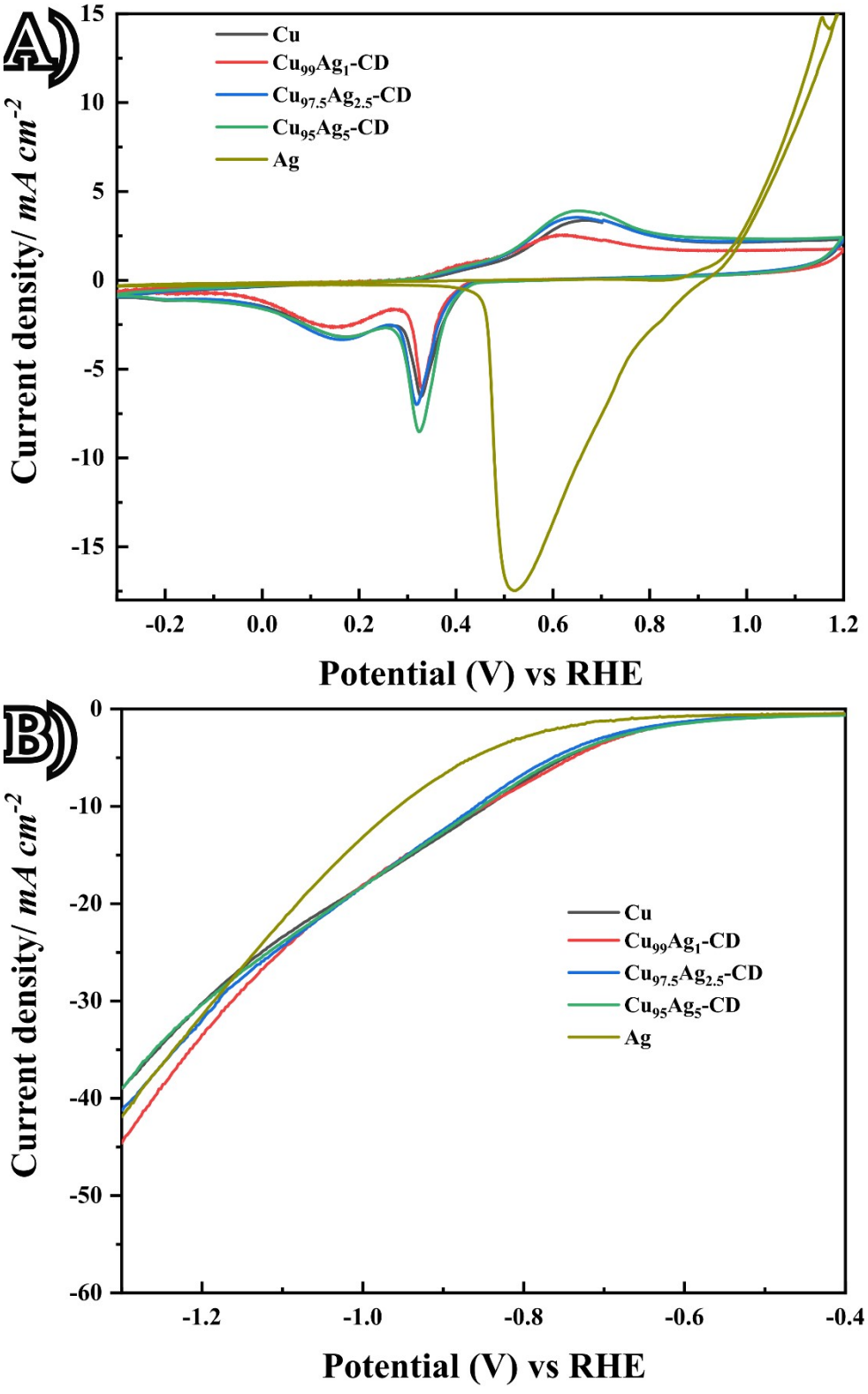

Fig. S13 A) CV and B) LSV comparison between bare Cu, Ag, $Cu_{99}Ag_1$-CD, $Cu_{97.5}Ag_{2.5}$-CD, and $Cu_{95}Ag_5$-CD.

Table S7. Overview of recently reported CuAg bimetallic catalysts for the eCO_2RR to C_{2+} products.

Catalyst	Electrolytic cell	Current density (mA cm^{-2})	$FE_{C_{2+}}$	$FE_{C_2H_4}$	FE_{EtOH}	$EE_{C_2H_4}$	EE_{EtOH}	Ref
$CuAg_{0.75}$ alloy	Flow	214	~65	35	21	21%	12.4%	1
Electrodeposited CuAg film	Flow	300	85	60	25	n.a.	n.a.	2
$Cu_{86}Ag_{14}$ alloy	Flow	250	~80	36	41	n.a.	25%	3
Ag NPs + Cu-Ag single-atom	Flow	720	94	38	47	n.a.	n.a.	4
Ag-Cu 5% core shells	Flow	300	80	22	53	n.a.	27%	5
Ag@Cu Np	Flow	30	/	41	/	39%	n.a.	6
Ag-decorated Cu_2O nanocubes	H-cell	10	63	32	17	37.3%	19.5%	7
Ag coated $Cu(OH)_2$ nanowires	Flow	350	~70	54	12	17.9%	4%	8
Cu@Ag core shell-NP	Flow	63	67.6	32.2	30.4	33.9%	31.2%	9
$Cu_{99}Ag_1$ – alloy thin film	Flow	150	75	42	24	28.7%	16.2%	This work

1. Tang, H., Liu, Y., Zhou, Y., Qian, Y. & Lin, B.-L. Boosting the Electroreduction of CO2 to Ethanol via the Synergistic Effect of Cu–Ag Bimetallic Catalysts. *ACS Appl. Energy Mater.* **5**, 14045–14052 (2022).
2. Hoang, T. T. H. *et al.* Nanoporous Copper–Silver Alloys by Additive-Controlled Electrodeposition for the Selective Electroreduction of CO_2 to Ethylene and Ethanol. *J. Am. Chem. Soc.* **140**, 5791–5797 (2018).
3. Li, Y. C. *et al.* Binding Site Diversity Promotes CO2 Electroreduction to Ethanol. *J. Am. Chem. Soc.* **141**, 8584–8591 (2019).
4. Du, C. *et al.* Cascade electrocatalysis via AgCu single-atom alloy and Ag nanoparticles in CO2 electroreduction toward multicarbon products. *Nat. Commun.* **14**, 6142 (2023).
5. Cai, Z. *et al.* Hierarchical Ag-Cu interfaces promote C-C coupling in tandem CO2 electroreduction. *Appl. Catal. B Environ.* **325**, 122310 (2023).
6. Hou, L. *et al.* Ag nanoparticle embedded Cu nanoporous hybrid arrays for the selective electrocatalytic reduction of CO2 towards ethylene. *Inorg. Chem. Front.* **7**, 2097–2106 (2020).
7. Herzog, A. *et al.* Operando Investigation of Ag-Decorated Cu2O Nanocube Catalysts with Enhanced CO2 Electroreduction toward Liquid Products. *Angewandte Chemie International Edition* **60**, 7426–7435 (2021).
8. Huang, Q., Wan, L., Ren, Q. & Luo, J. Elucidating the structure-activity relationship of Cu-Ag bimetallic catalysts for electrochemical CO2 reduction. *Journal of Energy Chemistry* **93**, 345–351 (2024).
9. Zhang, S. *et al.* Electrochemical Reduction of CO2 Toward C2 Valuables on Cu@Ag Core-Shell Tandem Catalyst with Tunable Shell Thickness. *Small* **17**, 2102293 (2021).

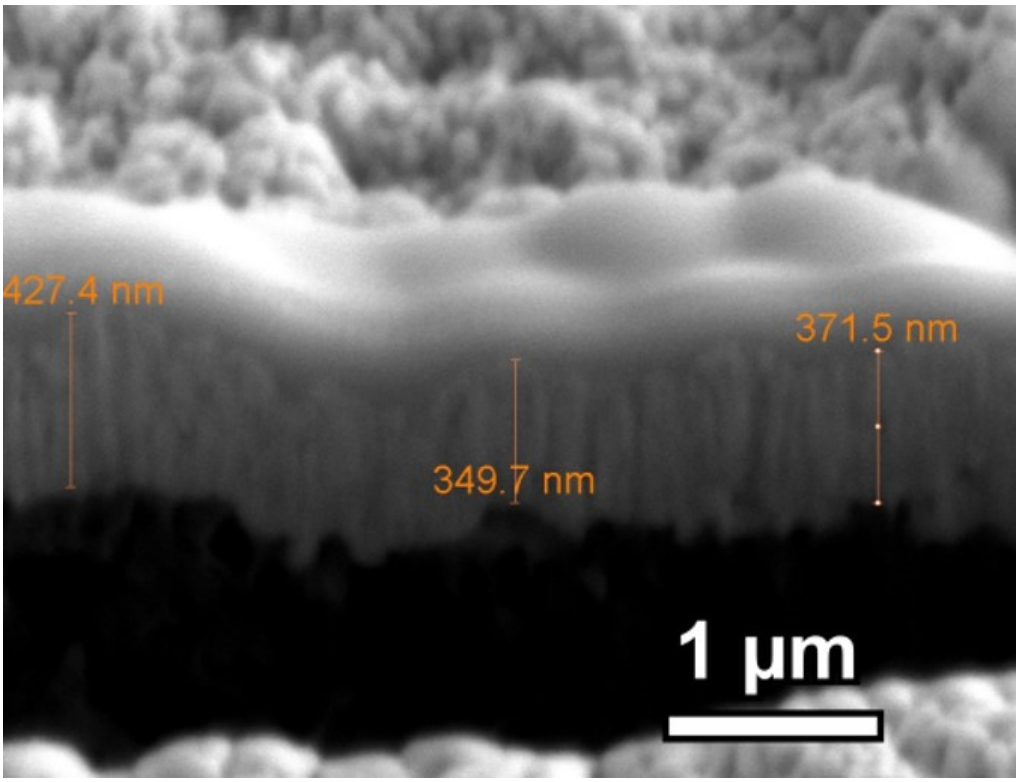

Fig. S14 FIB-SEM of $Cu_{99}Ag_1$ - CD, taken after electrolysis at J =150 mA cm^{-2} for 3 hours.

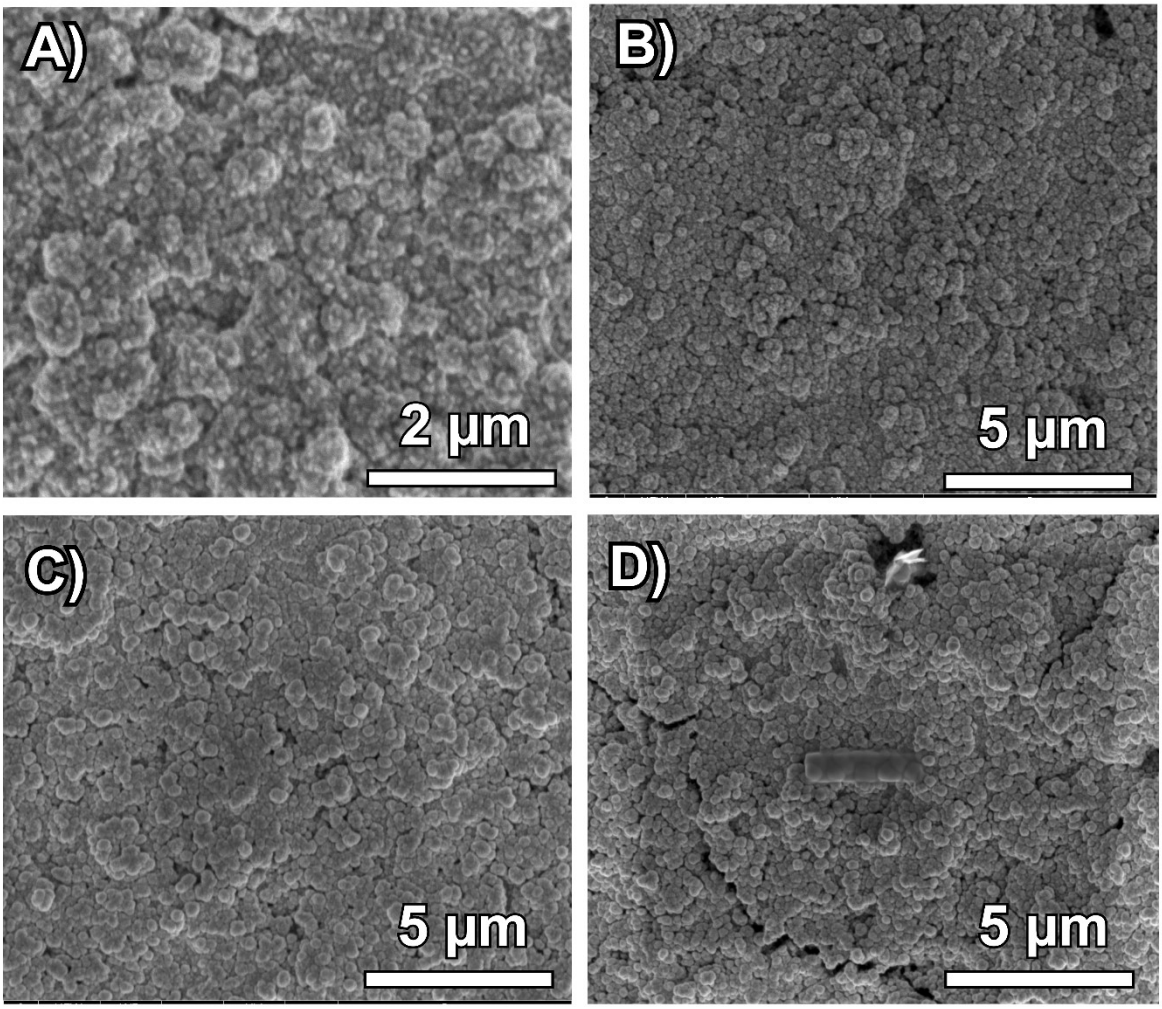

Fig. S15 SEM images from top view after electrolysis of J = 150 mA cm^{-2} of the different sputtered samples, with A) Cu 400 nm, B) $Cu_{90}Ag_{10}$ - L, C) $Ag_{10}Cu_{90}$ - L, and D) $Cu_{90}Ag_{10}$ – CD.

Fig. S16 Spent GDE with graphite holding plate, water droplets have permeated through the GDE.

Table S8. The measured C_{dl} of before and after electrolysis with the different $Cu_{100-x}Ag_x$ samples.

Sample	**C_{dl} (mF) before**	**C_{dl} (mF) after**	**Sample**	**C_{dl} (mF) before**	**C_{dl} (mF) after**	**Sample**	**C_{dl} (mF) before**	**C_{dl} (mF) after**
$Cu_{99}Ag_1$ - CD	2.71	**3.62**	**$Cu_{95}Ag_5$ - L**	**2.56**	**3.13**	**Ag_5Cu_{95} - L**	2.05	3.22
$Cu_{97.5}Ag_{2.5}$ - CD	2.51	**2.98**	**$Cu_{90}Ag_{10}$ - L**	**2.94**	**4.44**	**$Ag_{10}Cu_{90}$ - L**	1.89	2.80
$Cu_{95}Ag_5$ - CD	1.62	**4.28**	**$Cu_{85}Ag_{15}$ - L**	**2.05**	**4.08**	**$Ag_{15}Cu_{85}$ - L**	2	3.46
$Cu_{90}Ag_{10}$ - CD	3.1	**3.48**	**$Cu_{80}Ag_{20}$ - L**	**1.48**	**2.62**	**$Ag_{20}Cu_{80}$ - L**	2.57	3.22
$Cu_{85}Ag_{15}$ - CD	3.03	**3.20**				**Ag**	0.32	0.47
$Cu_{80}Ag_{20}$ - CD	1.93	**3.25**						

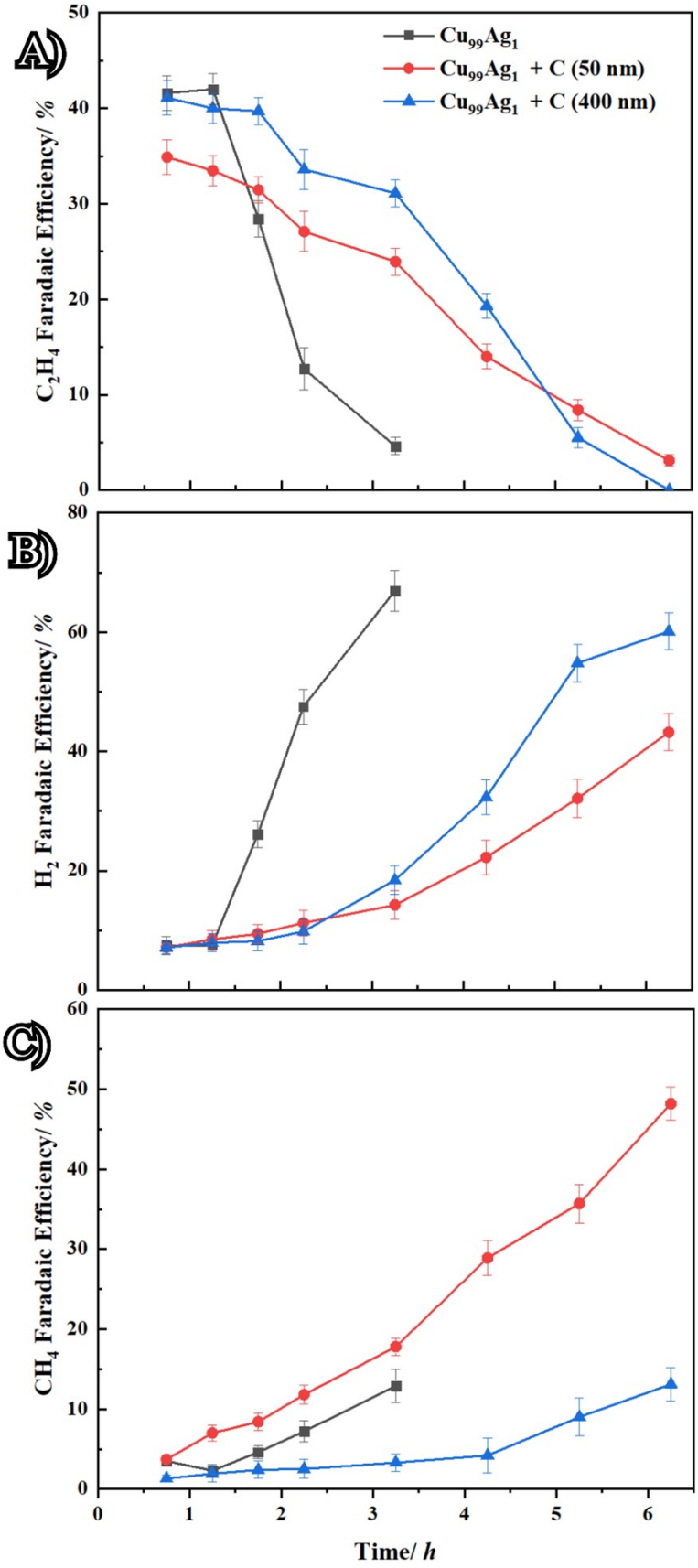

Fig. S17 The FE over 6 h stability measurement for respectively, A) C_2H_4, B) HER, and C) CH_4 for (black) bare $Cu_{99}Ag_1$, (red) $Cu_{99}Ag_1$ + C (50 nm), and (blue) $Cu_{99}Ag_1$ + C(400 nm). Error bars represent the deviation across three measurements.

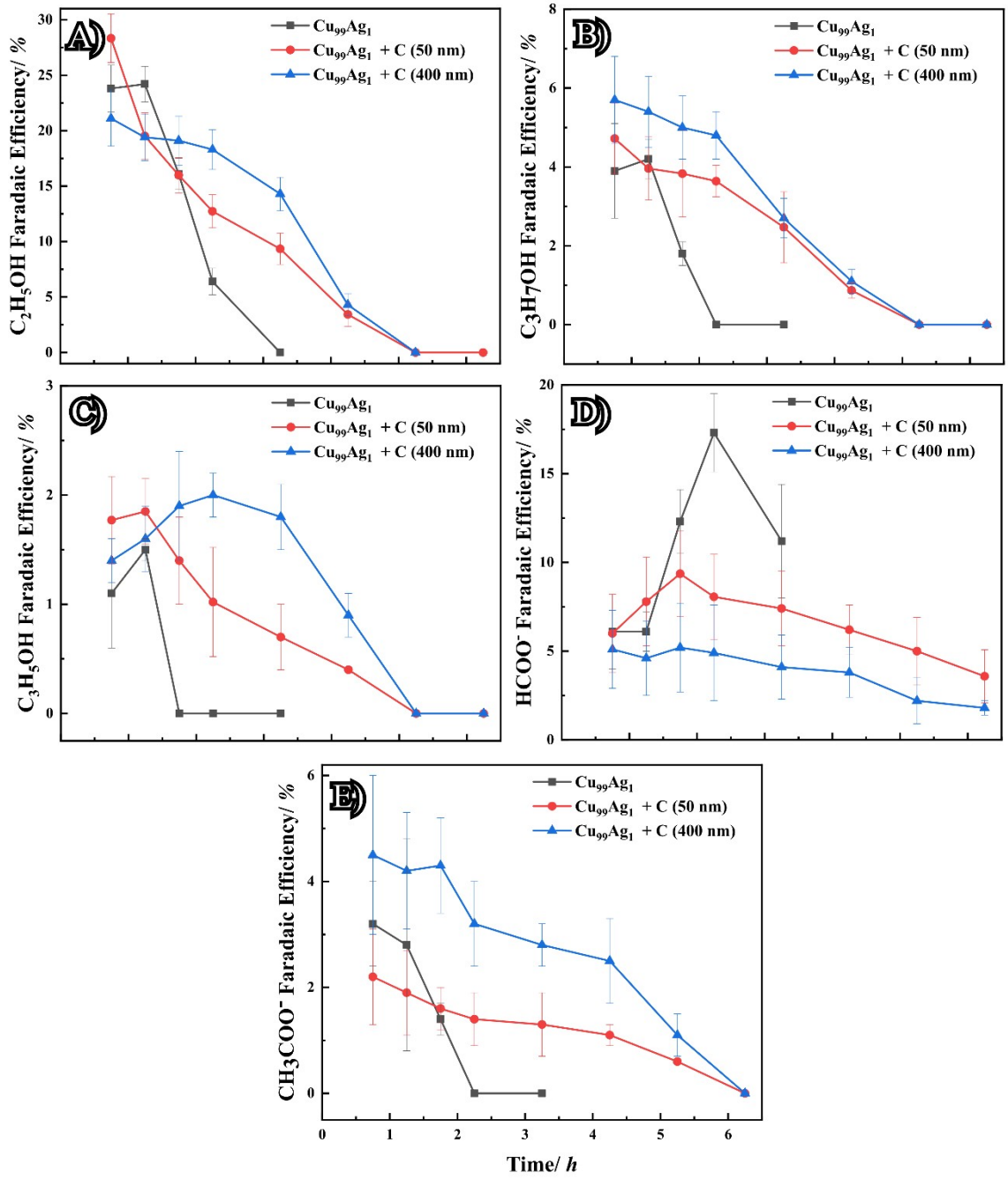

Fig. S18 Measured FEs for the liquid products A) C_2H_5OH, B) C_3H_7OH, C) C_3H_5OH, D) $HCOO^-$, and E) CH_3COO^-, during 6 h operation for $Cu_{99}Ag_1$-CD (black), $Cu_{99}Ag_1$-CD + C (50 nm) (red), and $Cu_{99}Ag_1$-CD + C (400 nm) (blue). Error bars represent the deviation across three measurements.

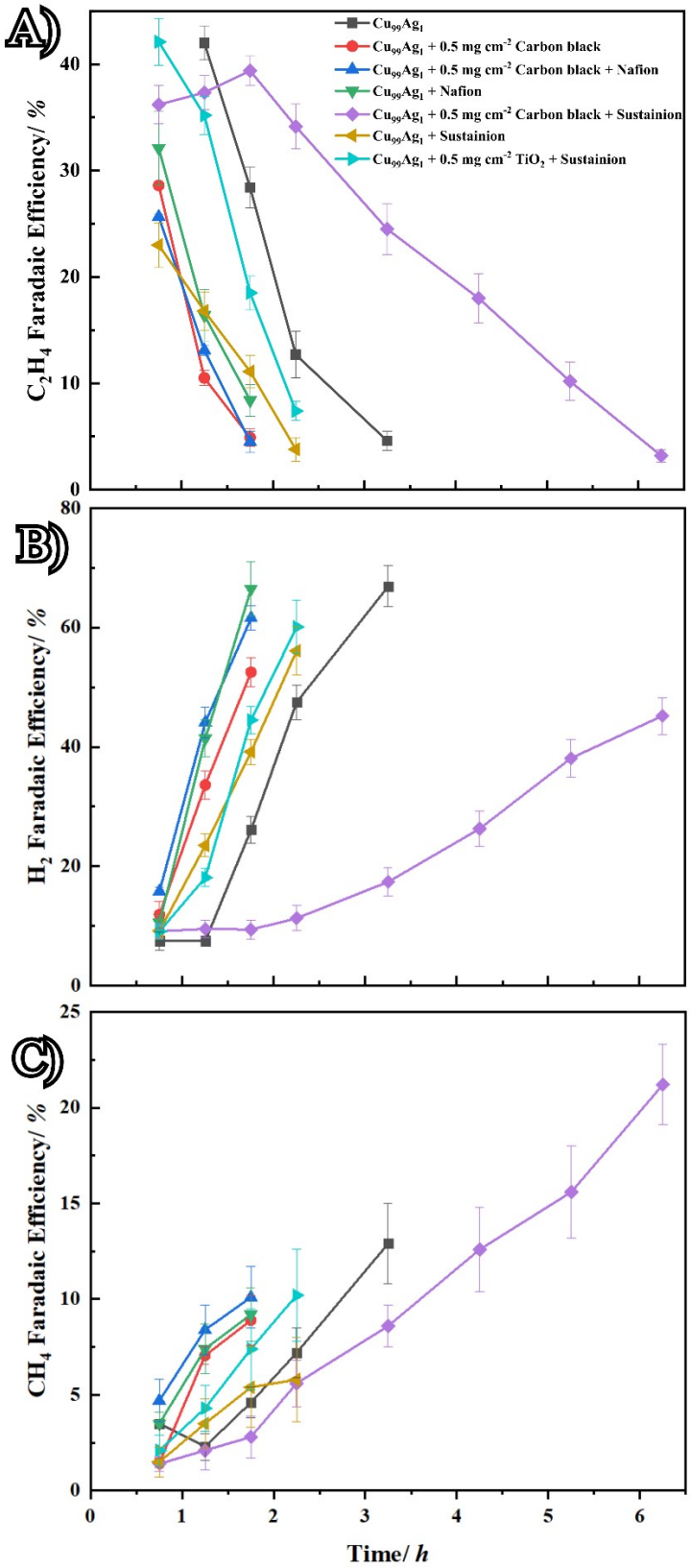

Fig. S19 The FE over 6 h stability measurement for respectively, A) C_2H_4, B) HER, and C) CH_4 for (black) bare $Cu_{99}Ag_1$ (black), $Cu_{99}Ag_1$+ 0.5 mg cm^{-2} Carbon black (red), $Cu_{99}Ag_1$ + 0.5 mg cm^{-2} Carbon black + Nafion (blue), $Cu_{99}Ag_1$ + Nafion (green), $Cu_{99}Ag_1$ + 0.5 mg cm^{-2} Carbon black + Sustainion (purple), $Cu_{99}Ag_1$ + Sustainion (yellow), $Cu_{99}Ag_1$ + 0.5 mg cm^{-2} TiO_2 + Sustainion (cyan). Error bars represent the deviation across three measurements.

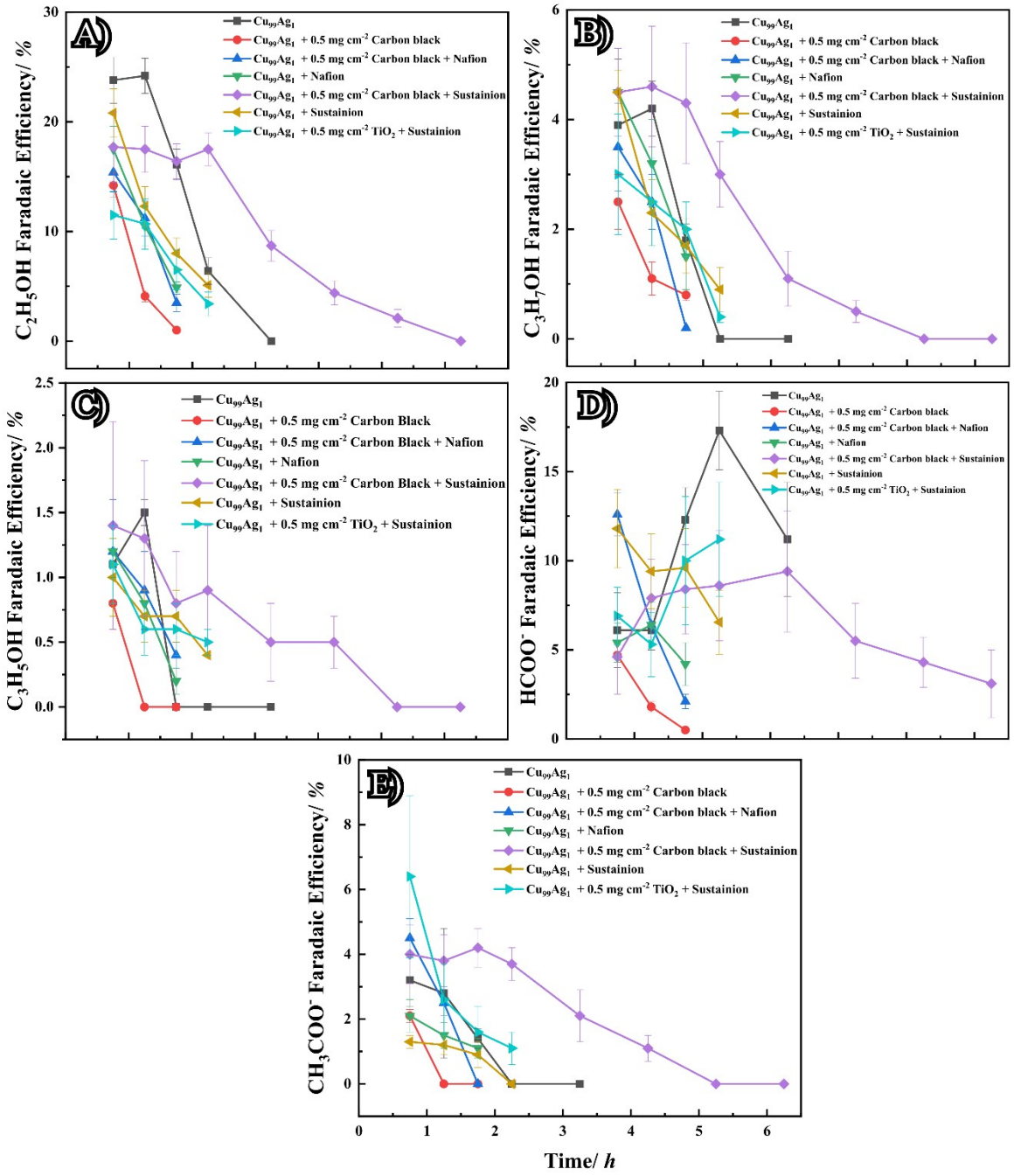

Fig. S20 Measured FEs for the liquid products A) C_2H_5OH, B) C_3H_7OH, C) C_3H_5OH, D) $HCOO^-$, and E) CH_3COO^-, during 6 h operation for $Cu_{99}Ag_1$ (black), $Cu_{99}Ag_1$ + 0.5 mg cm^{-2} Carbon black (red), $Cu_{99}Ag_1$ + 0.5 mg cm^{-2} Carbon black + Nafion (blue), $Cu_{99}Ag_1$ + Nafion (green), $Cu_{99}Ag_1$ + 0.5 mg cm^{-2} Carbon black + Sustainion (purple), $Cu_{99}Ag_1$ + Sustainion (yellow), and $Cu_{99}Ag_1$ + 0.5 mg cm^{-2} TiO_2 + Sustainion (cyan). Error bars represent the deviation across three measurements.

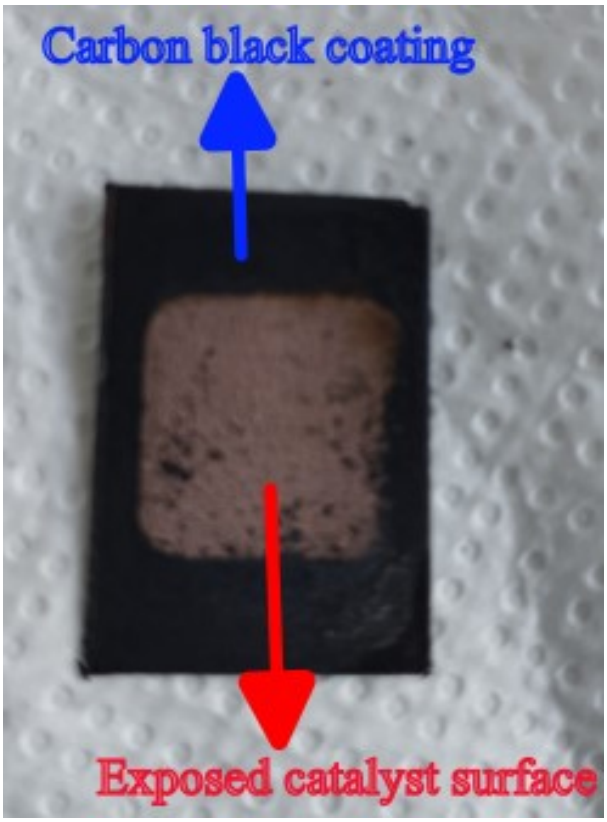

Fig. S21 Spent $Cu_{99}Ag_1$-CD with carbon black coating, after electrolysis, the carbon black is beginning to detach.

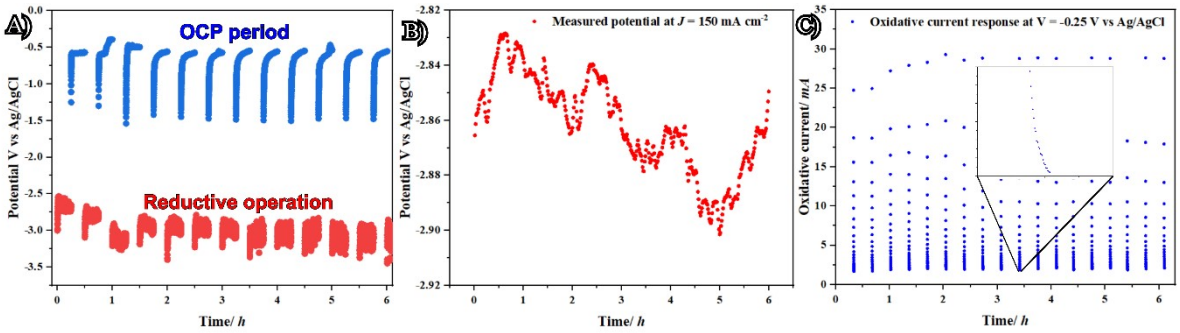

Fig. S22 During p-eCO2RR for A) Time-dependent potential 15 min of 'on' and 15 min of OCP period, B) potential response during 15 min 'on' reductive current, and C) oxidative current response when applying an oxidative pulse of -0.25 V vs Ag/AgCl for 30 s.

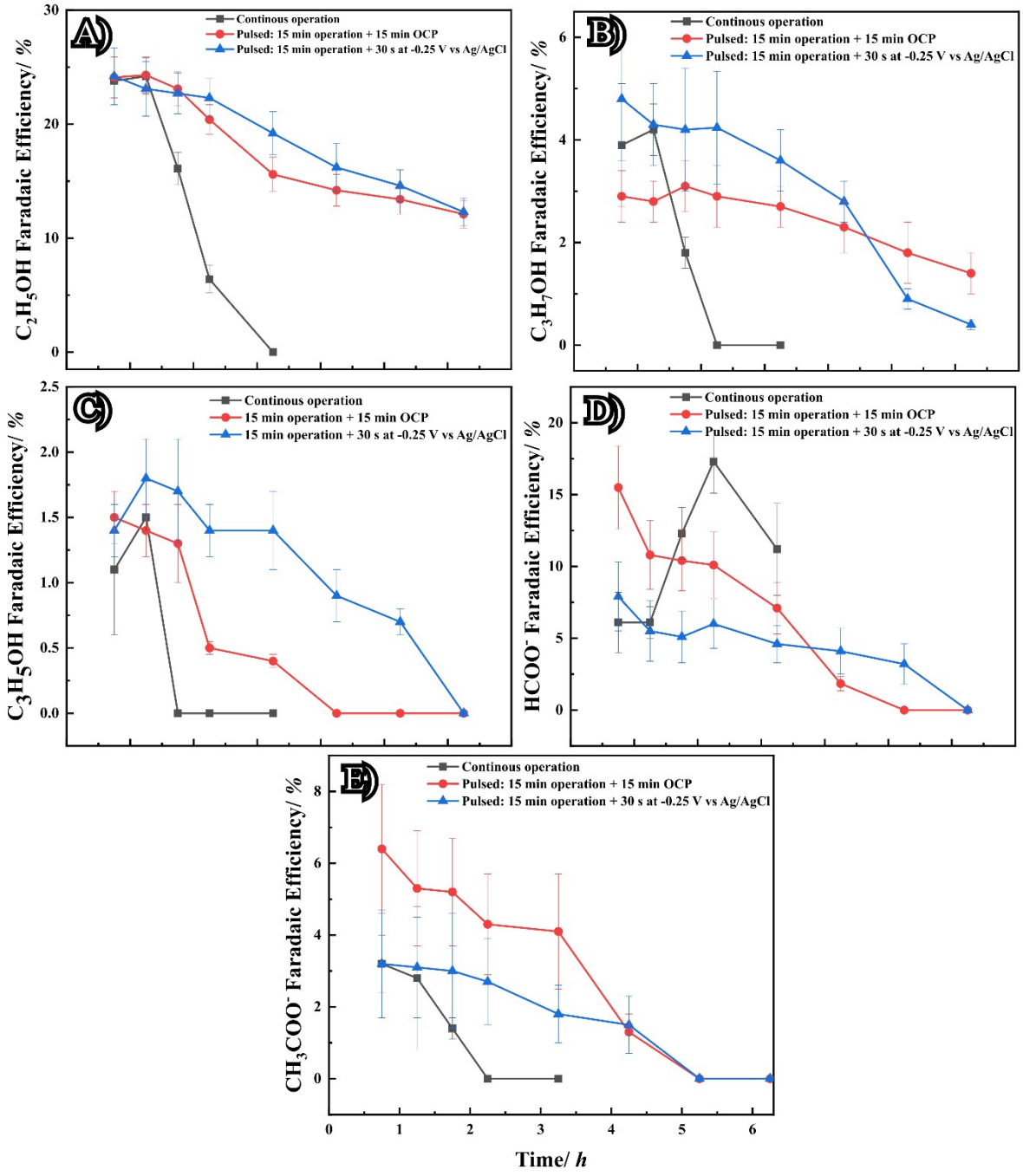

Fig. S23 Measured FEs for the liquid products A) C_2H_5OH, B) C_3H_7OH, C) C_3H_5OH, D) $HCOO^-$, and E) CH_3COO^-, during 6 h operation for $Cu_{99}Ag_1$ at continuous operation (black), Pulsed: 15 min operation + 15 min OCP (red), and Pulsed: 15 min operation + 30 s at -0.25 V vs Ag/AgCl (blue). Error bars represent the deviation across three measurements.